Marine and Petroleum Geology 44 (2013) 71–81

Contents lists available at SciVerse ScienceDirect

Marine and Petroleum Geology

journal homepage: www.elsevier.com/locate/marpetgeo

Tracing the evolution of seep fluids from authigenic carbonates: Green Canyon, northern Gulf of Mexico

Youyan Bian [a,d], Dong Feng [b,*], Harry H. Roberts [c], Duofu Chen [a,b,*]

[a] CAS Key Laboratory of Marginal Sea Geology, Guangzhou Institute of Geochemistry, Chinese Academy of Sciences, Guangzhou 510640, China
[b] CAS Key Laboratory of Marginal Sea Geology, South China Sea Institute of Oceanology, Chinese Academy of Sciences, Guangzhou 510301, China
[c] Coastal Studies Institute, Department of Oceanography and Coastal Sciences, School of the Coast and Environment, Louisiana State University, Baton Rouge, LA 70803, USA
[d] University of Chinese Academy of Sciences, Beijing 100049, China

ARTICLE INFO

Article history:
Received 15 January 2013
Received in revised form
18 March 2013
Accepted 25 March 2013
Available online 6 April 2013

Keywords:
Authigenic carbonate
Cold seep
Carbon and oxygen isotope
^{14}C dating
Gulf of Mexico

ABSTRACT

Authigenic carbonates from hydrocarbon seeps are unique long-term archives of past fluid flow. The studied samples were collected from Green Canyon block 140 at a water depth of 260 m in the Gulf of Mexico. Petrography, X-ray diffraction, stable isotopes and ^{14}C dating were applied to assess the evolution of seep activity and potential driving forces. The carbonates are dominated by high-Mg calcite (HMC) and aragonite, with a minor amount of low-Mg calcite (LMC) and dolomite. Petrographically, peloids, clotted microfabric, acicular aragonite and a variable content of bioclasts were observed. Three types of carbonates are recognized. Structure I carbonates, with ^{14}C ages from 46.5 ka to 25.8 ka BP, are characterized by δ^{13}C values from −23.2‰ to 5.1‰, suggesting multiple carbon sources that include thermogenic methane, biodegraded crude oil, seawater and residual CO_2 from methanogenesis at greater depth. In contrast, Structure II carbonates formed between 17.6 ka and 11.7 ka BP and have δ^{13}C values varying from −22.2‰ to −8.8‰, suggesting carbon sources similar to those of Structure I carbonates but with a negligible influence of residual CO_2 from methanogenesis. In addition, the presence of LMC in this type of carbonate may be associated with brine seepage. Structure III carbonates among the youngest of the samples analyzed with ^{14}C ages of 1.2 ka BP. These carbonates have the most negative δ^{13}C values ranging from −36.1‰ to −26.8‰, suggesting that thermogenic methane is the primary carbon source. The majority carbonates of both Structure I and II are slightly ^{18}O-enriched, which is most likely related to the incorporation of water from dehydration of clay minerals. The considerable range of mineralogical and isotopic variations of the studied carbonates highlights the local control of the seepage flux. It is proposed that factors affecting the activity of hydrocarbon seeps are sea level changes and salt movement. The combination of petrography, stable isotopes, and dating approach used here, highlights that these are valuable tools to assess the variability of past fluid flow at hydrocarbon seeps.

1. Introduction

Cold hydrocarbon seepage is a frequently observed phenomenon in marine settings worldwide (e.g., Campbell, 2006; Judd and Hovland, 2007 and references therein). The key process at cold seeps is anaerobic oxidation of methane, conjointly operated by consortia of anaerobic methane-oxidizing archaea and sulfate-reducing bacteria (Boetius et al., 2000; Valentine and Reeburgh, 2000). This process leads to an increase of pore water alkalinity by the production of bicarbonate that favors the precipitation of authigenic carbonates (Baker and Burns, 1985; Berner, 1980), the so-called seep carbonates or methanogenic carbonates. Seep carbonates, thus, provide excellent long-term archives of past seepage and associated environmental parameters (Aloisi et al., 2000; Birgel et al., 2011; Bohrmann et al., 1998; Chen et al., 2006; Feng et al., 2009a, 2010b; Greinert et al., 2001, 2002; Greinert and Derkachev, 2004; Mazzini et al., 2004, 2008; Naehr et al., 2007; Peckmann et al., 1999, 2001a,b, 2002, 2009; Tong et al., 2013).

Seep carbonates are known to show complex mineralogical as well as carbon and oxygen isotopic compositions (Campbell, 2006; Gieskes et al., 2005; Mazzini et al., 2005; Naehr et al., 2007; Peckmann et al., 1999, 2001a,b; Peckmann and Thiel, 2004;

* Corresponding authors. Tel.: +86 20 85290286; fax: +86 20 85290130.
E-mail addresses: bianyouyan@gig.ac.cn (Y. Bian), feng@scsio.ac.cn (D. Feng), hrober3@lsu.edu (H.H. Roberts), cdf@gig.ac.cn (D. Chen).

0264-8172/$ – see front matter © 2013 Elsevier Ltd. All rights reserved.
http://dx.doi.org/10.1016/j.marpetgeo.2013.03.010

Roberts et al., 2010; Roberts and Aharon, 1994). Carbonate minerals in seep carbonates are primarily high-Mg calcite (HMC), aragonite and dolomite (protodolomite; Greinert et al., 2001; Naehr et al., 2007; Peckmann et al., 2001b; Roberts et al., 2010; Roberts and Aharon, 1994). Many factors influence the type of carbonate minerals that precipitate at hydrocarbon seeps. In general, high levels of carbonate supersaturation in combination with a high sulfate concentration seem to favor aragonite precipitation over HMC and dolomite (Greinert et al., 2001; Moore et al., 2004; Naehr et al., 2000, 2007; Peckmann et al., 2001b). The occurrence of low-Mg calcite (LMC) may be attributed to a brine-rich environment, which is relatively Mg-depleted compared to normal marine settings that usually produce HMC and aragonite (cf. Aloisi et al., 2000; Davis, 2000; Feng and Roberts, 2011; Judd and Hovland, 2007).

The $\delta^{13}C$ values of seep carbonates reflect the isotopic signature of the dissolved inorganic carbon pool at the time of carbonate precipitation (Mazzini et al., 2004, 2008; Naehr et al., 2007; Peckmann and Thiel, 2004; Roberts and Aharon, 1994). At seeps, the possible carbon sources include: 1) biogenic methane ($\delta^{13}C < -65‰$; Whiticar, 1999) and thermogenic methane ($\delta^{13}C = -50‰$ to $-30‰$; Sackett, 1978; Whiticar et al., 1986), 2) oil fraction ($\delta^{13}C = -35‰$ to $-25‰$; Roberts and Aharon, 1994), 3) seawater ($\delta^{13}C = 0 \pm 3‰$; Anderson and Arthur, 1983), and 4) residual CO_2 from methanogenesis ($\delta^{13}C$ as high as 26‰; Gieskes et al., 2005; Naehr et al., 2007; Paull et al., 2007). The stable oxygen isotopic compositions of a specific carbonate mineral phase depend on the formation temperature and isotopic composition of the source water where the precipitation occurred (Friedman and O'Neil, 1977; Naehr et al., 2000, 2007). Anomalously positive $\delta^{18}O$ values may be derived from decomposition of gas hydrate or dehydration of clay minerals (e.g., Bohrmann et al., 1998; Davidson et al., 1983; Hesse, 2003; Matsumoto, 1994). Samples that are ^{18}O-depleted may indicate the influence of the local presence of meteoric water or residual fluids from gas hydrate formation during carbonate precipitation (Dahlmann and de Lange, 2003; Greinert et al., 2001).

Seafloor observations indicate that the physical, chemical and biological processes at hydrocarbon seeps can change significantly with time (Chen et al., 2004; Greinert, 2008; Roberts, 2001; Roberts and Carney, 1997; Schneider von Deimling et al., 2011; Solomon et al., 2008; Torres et al., 2002; Tryon, 2004; Tryon and Brown, 2001), and this temporal variability can be expressed by the difference in geochemical and mineralogical signatures of the associated seep carbonates (Bayon et al., 2007, 2011; Campbell et al., 2010; Díaz-del-Río et al., 2003; Feng et al., 2009a,b, 2010a; Ivanov et al., 2010; Magalhães et al., 2012; Mazzini et al., 2006, 2008; Naehr et al., 2007; Peckmann et al., 2001b, 2009; Pierre et al., 2012; Rongemaille et al., 2011). Here, we investigated authigenic carbonate rocks from the subsurface sediment of the hydrocarbon seeps at Green Canyon block 140 (GC140) of the Gulf of Mexico (GOM) continental slope. Petrography, mineralogy, stable isotopes and ^{14}C dating were applied to constrain the conditions under which the carbonates formed. The obtained data were also used to constrain the long-term evolution of the seep fluids and the possible driving forces. This study aims at tracing the evolution of seep fluids by a multidisciplinary study of authigenic carbonates.

2. Geological setting and sampling

The Gulf of Mexico is a hydrocarbon-bearing basin with various types of salt structures. Faults resulting from subsurface salt movement serve as pathways for deep hydrocarbon migration. The hydrocarbon seepage produces brine pools, gas hydrates and authigenic carbonates (MacDonald et al., 2010; Milkov and Sassen, 2001; Roberts et al., 2000, 2010; Sassen et al., 1999; Weimer et al., 1998). The GC140 seep site is located in the northern upper continental slope of the GOM (Fig. 1). This area is characterized by an abundance of faults activated by salt diapirism. Geophysical data, submersible observations, and samples retrieved clearly indicate

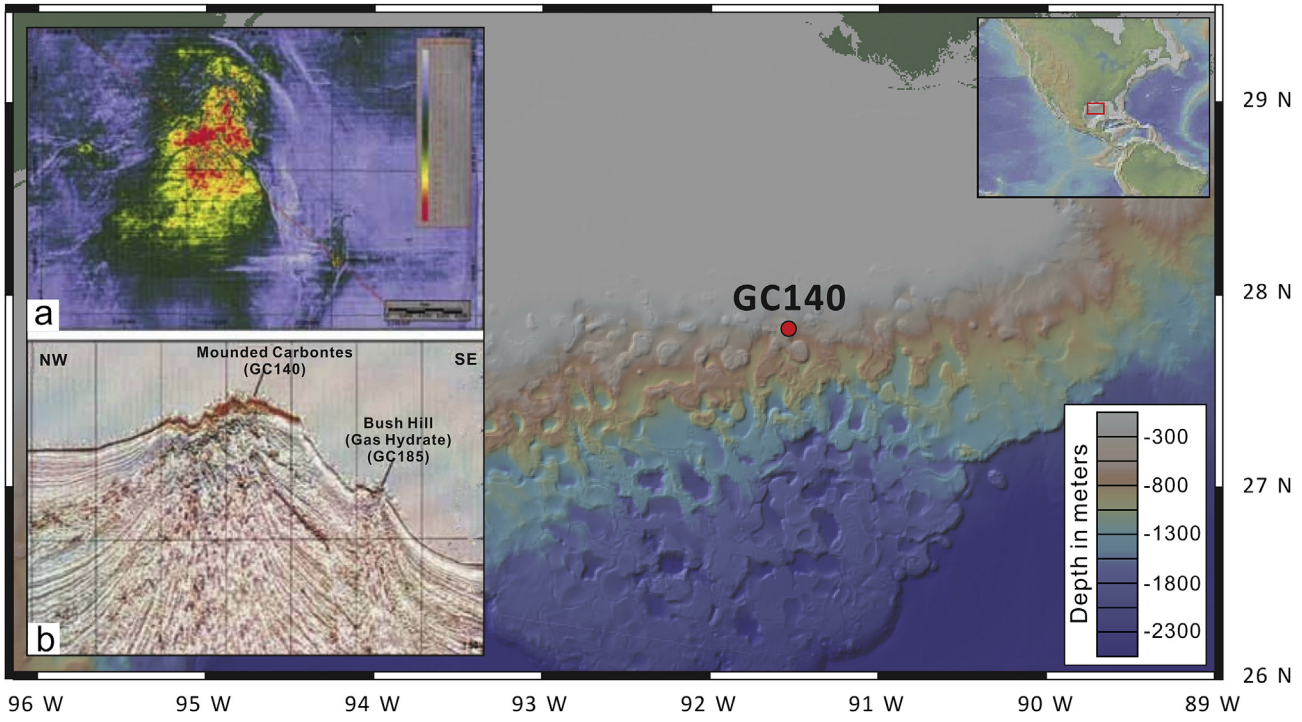

Figure 1. Location of the Green Canyon block 140 (27°48′N/91°32′W) study site, northern Gulf of Mexico. The inset 3-D seismic surface amplitude illustrates the extent of the hard bottom (a) and the profile view (b), showing that the dome top has an irregular surface and that the seafloor reflector is a strong, positive reflector, indicating a hard bottom (Roberts, 2011).

that the crestal areas of the GC140 dome are characterized by linear patterns of authigenic seep mounds, which are mainly controlled by faults (Roberts, 2001, 2011). The mound-like buildups, 20–100 m in diameter and up to 20 m in height, are composed of chaotically oriented blocks and clasts with a high proportion of clasts and biological detritus in the surrounding sediments (Aharon, 1994; Roberts et al., 1990, 2000; Roberts and Aharon, 1994).

Bathymetric and high resolution seismic profiles and side-scan sonographs clearly indicate that the thin sedimentary sequence over the shallow salt mass of GC140 is broken by numerous faults and that most mounded carbonates are cut due to salt deformation (Roberts et al., 2000; Roberts and Carney, 1997). Submarine observation showed that micro-seepage is currently occurring at GC140 and further analysis revealed that the seep fluid mainly consists of thermogenic gas from a deep reservoir with $\delta^{13}C$ values $\sim -46‰$ (Roberts et al., 2000; Roberts and Aharon, 1994; Sassen et al., 2004). The studied authigenic carbonates were recovered during Johnson-Sea-Link dive 2591 in 1989. All samples were collected from the shallow subsurface (<50 cm below the seafloor). The water depth at the site was 260 m, and the bottom water temperature was 12.87 °C. Scattered living tube worms and sponges were present at the sampling site.

3. Methods

The samples were washed with fresh water and air dried after collection. Typical samples were selected to make thin sections. The thin sections were observed using a LEICA-DMRX optical microscope. The microstructure of the seep carbonate was examined on freshly fractured surfaces using a scanning electron microscope (SEM). The samples were platinum coated (20 s) prior to the SEM observation. Photographs were taken using a HITACHI S-4800 SEM operating at 2.0 kV with a 7–13 mm working distance. The elementary composition was analyzed by a HORIBA EX-250, which is housed in the Guangzhou Institute of Energy Conversion, Chinese Academy of Sciences (CAS). The bulk mineralogy and the relative abundance of carbonate minerals were determined by X-ray diffraction (XRD) using a Rigaku DXR 3000 computer-automated diffractometer at Guangzhou Institute of Geochemistry (GIG), CAS. Samples for XRD analyses were crushed into powder less than 200 mesh using an agate mortar and pestle. The X-ray source was a Cu anode operated at 40 kV and 40 mA using CuKα radiation equipped with a diffracted beam graphite monochromator. The samples were scanned at an interval of 5–65° (2θ) with a step size of 0.02° and a count time of 5 s per step. The diverging, scattering, and receiving slits were 0.5°, 0.5°, and 0.15 mm, respectively. The relative proportions of different carbonate minerals were quantified on the basis of the (104) peak areas of calcite, Mg-calcite, and dolomite and the (111) peak areas of aragonite using calibration curves (Greinert et al., 2001). The position of the (104) peak was used to determine the Mg content of carbonate minerals (Goldsmith et al., 1961; Lumsden, 1979). Calcite with less than 5 mol % $MgCO_3$ was considered as LMC, and calcite compositions of 5–20 mol% $MgCO_3$ were referred to HMC (Burton and Walter, 1991). Carbonate phases with 30–50 mol% $MgCO_3$ were classified as dolomite (Burton, 1993).

The samples for carbon and oxygen isotope analyses were taken from carbonate rocks with a hand-held dental drill. The powdered samples were processed with 100% phosphoric acid at 90 °C to release CO_2 for analysis using a GV Isoprime II stable isotopic mass spectrometer at State Key Laboratory of Isotope Geochemistry, CAS. All isotope values are expressed using the δ-notion relative to the Vienna-PeeDee Belemnite (V-PDB) standard. The values were reported in permil (‰) with a standard deviation of less than 0.1‰ (2σ) for the $\delta^{13}C$ values and 0.2‰ (2σ) for the $\delta^{18}O$ values.

The ^{14}C measurements were performed on shell fragments cemented in the carbonate matrix. To remove contaminants, the shell fragments were carefully stripped of adhering sediments with a micro drill, soaked in water with 0.5 M HCl to remove residual carbonate cement, washed with distilled water repeatedly until neutral and then freeze-dried for 24 h under vacuum. The cleaned samples were reacted with 100% phosphoric acid at room temperature for 48 h. The purified CO_2 gas was reduced to obtain graphite targets by sealed tube zinc reduction method (Xu et al., 2007). The pretreatment and preparation of graphite targets was finished at the AMS-^{14}C Lab at GIG, CAS. The graphite targets were measured at the State Key Laboratory of Nuclear Physics and Technology (Peking University, AMS facility) with an analytical precision better than 5‰. The ^{14}C ages were calculated as years before present (BP, years from 1950 AD) using CALIB 5.0. The errors were expressed as $\pm 1\sigma$.

4. Results

4.1. Mineralogy and petrography

The carbonate samples show no obvious stratification and present as irregular structures. The carbonate mineralogies are summarized in Table 1. The carbonate contents vary between 74 wt% and 97 wt%. Based on their different morphologies cement types, the authigenic carbonates were classified into three types: Structure I, Structure II, and Structure III (Fig. 2).

Structure I carbonates are mainly composed of nodules and matrix. The dominant mineral present is HMC in the form of nodules. The nodules occur as homogenous micrite while the matrix is characterized by a co-occurrence of microcrystalline Mg-calcite, fibrous aragonite and bioclasts (less than 5%; Figs. 3a, b and 4a, b). Fan-shaped aragonite aggregates developed in the inner wall of the shells (Fig. 3c). Framboidal pyrites are common and usually dispersed in the matrix (Figs. 3j and 4c).

Structure II carbonates are semi-consolidated and contain abundant bioclasts (up to 30% of the volume). The carbonates are typically composed of HMC and aragonite, followed by LMC. Foraminifers and bivalve fragments are the dominant biogenic components (Fig. 3d). The matrix is dominated by microcrystalline Mg-calcite and acicular aragonite (Fig. 3e–g). Well-developed Mg-calcite and NaCl crystals were frequently observed in the matrix (Fig. 4d, e).

Structure III carbonates have a dense homogenous microcrystalline structure with a small number of bioclasts. Aragonite is the dominant carbonate mineral phase, followed by HMC. Aragonite is frequently present as microcrystalline matrix and acicular cement in pore spaces (Fig. 4f). Clotted microfabric with hazy structure

Table 1
Mineral composition of the seep carbonates.

Sample no.	LMC (Mg%)	HMC (Mg%)	Arag.	P/dolo.	Qtz	Illite	Kaolinite	Feldspar
Structure I carbonates								
4-a	–	53.8(10)	18.3	2.0	6.7	5.4	2.5	11.3
B-9	–	27.8(12)	53.1	2.3	7.5	5.8	2.9	0.6
B-10	9.8(0)	35.1(13)	47.1	–	4.1	3.3	–	0.6
Structure II carbonates								
B-11	12.5(0)	27.4(14)	54.2	–	3.4	2.5	–	–
B-12	11.0(1)	15.5(14)	70.4	–	3.1	–	–	–
B-3	11.3(0)	41.9(13)	43.0	–	2.4	1.4	–	–
Structure III carbonates								
F-2	–	15.0(18)	74.5	–	5.3	3.6	–	1.6

Minerals: Qtz = quartz, LMC = low-Mg calcite, HMC = high-Mg calcite, Arag. = aragonite, P/dolo. = protodolomite/dolomite, Mg% = mol% $MgCO_3$ in carbonate minerals.

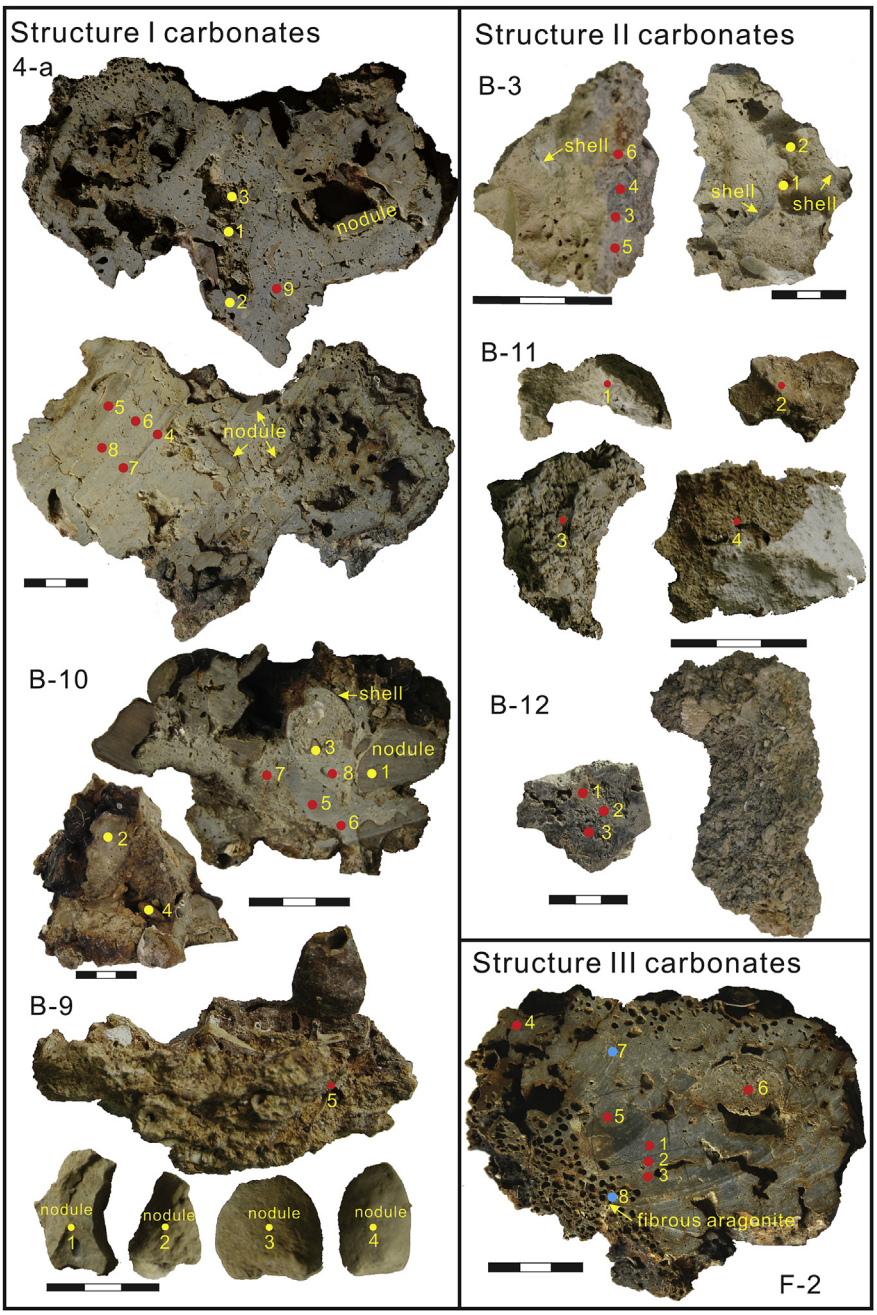

Figure 2. Morphologies and sampling points for the stable isotope data of seep carbonates. The results of the stable isotope analysis are listed in Table 2. Yellow dots represent nodules, red dots represent matrix, and blue dots represent pore fillings. Samples 4-a and B-10 of Structure I carbonates are mainly composed of brown dense nodules and gray matrix. B-9 of Structure I carbonates is composed of multiple scattered nodules. B-3, B-11 and B-12 of Structure II carbonates are composed of high content of bioclasts cemented by matrix. All scale bars are 3 cm. (For interpretation of the references to color in this figure legend, the reader is referred to the web version of this article.)

cemented by sparitic aragonite is one of the typical carbonates fabrics in Structure III (Figs. 3h, i).

4.2. Carbon and oxygen isotopic compositions

The carbon and oxygen isotopic compositions of the three structures vary widely (Table 2; Fig. 5). The $\delta^{13}C$ values of the Structure I carbonates vary between −23.2‰ and 5.1‰. The stable oxygen isotopic compositions of these samples are between 2.2‰ and 3.4‰. The $\delta^{13}C$ and $\delta^{18}O$ values of Structure II carbonates range from −22.2‰ to −8.8‰ and 2.0‰–3.5‰, respectively. The stable isotopic values of the Structure III carbonates display relatively narrow ranges, with $\delta^{13}C$ values from −36.1‰ to −26.8‰ and $\delta^{18}O$ values from 1.9‰ to 2.7‰.

4.3. ^{14}C ages

Bivalve shell materials cemented in the seep carbonates have ^{14}C ages between 46.5 ka and 1.2 ka BP (Table 3). The ^{14}C ages of the Structure I carbonates vary between 46.5 ka and 25.8 ka BP while the ^{14}C ages of the Structure II carbonates range from 17.6 ka to 11.7 ka BP. The Structure III carbonates have the youngest ^{14}C ages of approximately 1.2 ka BP. One exception is sample B-10 with ^{14}C ages from 41.3 ka to 5.0 ka BP. The carbon isotopic values of the

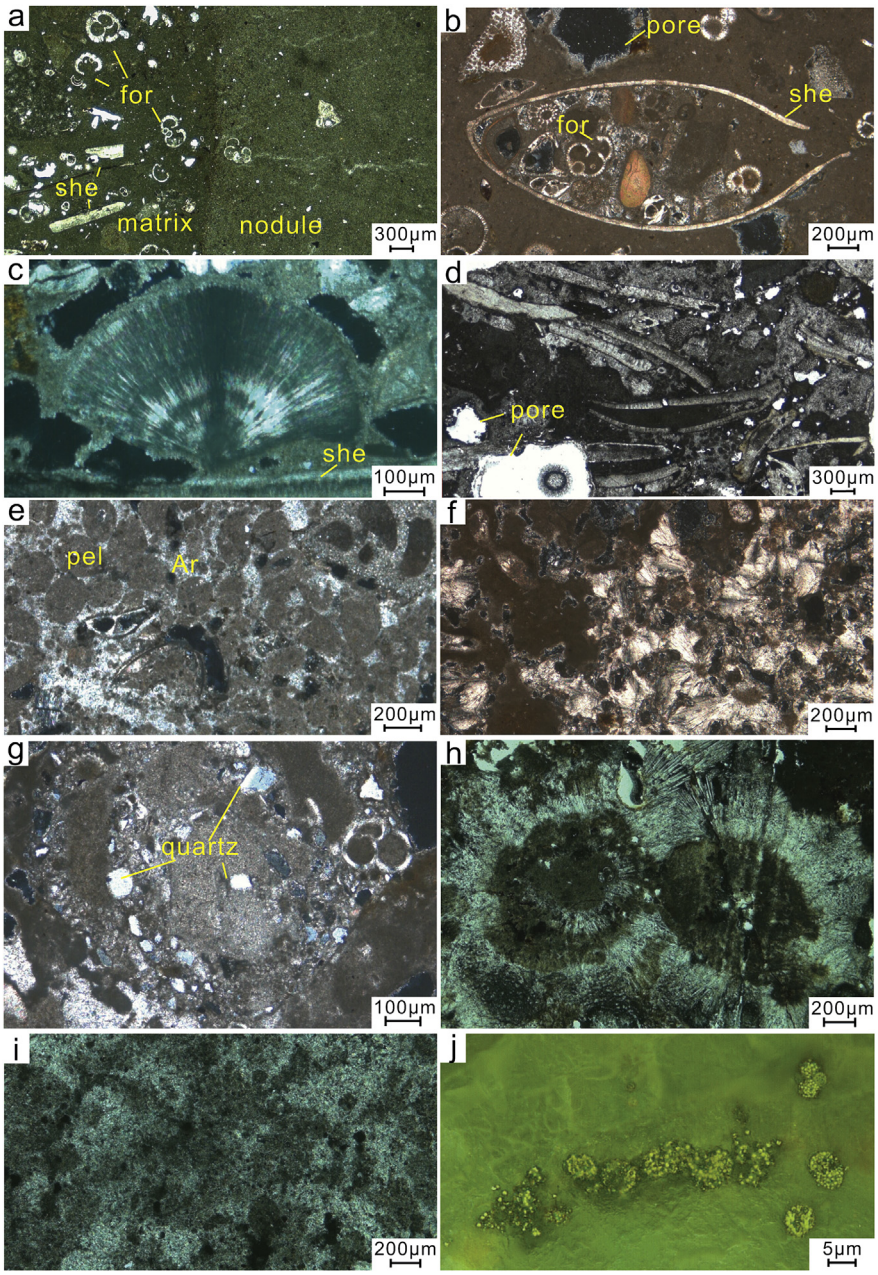

Figure 3. Photomicrographs of GC140 seep carbonates. (a) Structure I carbonates are composed of microcrystalline nodules and matrix with a low content of bioclasts (for, foraminifer; she, bivalve shell fragments), sample B-10, plane polarized light. (b) The co-occurrence of bivalve shells and foraminifer in the matrix of 4-a of Structure I carbonates, cross polarized light. (c) Fan-shaped aragonite originated from the shell wall, B-10 of Structure I carbonates, cross polarized light. (d) Structure II carbonates contain a high content of fragmented bivalve shells (up to 30%), sample B-11, plane polarized light. (e) Circumgranular sparitic aragonite (labeled "Ar") cement around spheric or elliptical, micritic peloids (labeled "pel"), B-3 of Structure II carbonates, plane polarized light. (f) A co-occurrence of acicular aragonite crystals (lower right) and micritic matrix (upper left), B-12 of Structure II carbonates, cross polarized light. (g) Microcrystalline matrix with a high content of quartz in B-3 of Structure II carbonates, plane polarized light. (h) Radial aragonite developed in F-2 of Structure III carbonates, plane polarized light. (i) The clotted microfabric preserved in carbonates has an irregular shape and unclear margin, cemented by sparitic aragonite, sample F-2, plane polarized light. (j) Framboidal pyrites approximately 0.5 μm in diameter dispersed in the matrix of B-10 of Structure I carbonates, reflected light.

studied shells vary from −2.9‰ to 3.8‰, suggesting that the ^{14}C ages are reliable (cf. Aharon et al., 1997; Paull et al., 1989; Peckmann et al., 2001b).

5. Discussion

5.1. Formation condition and fluid source

The mineral composition of seep carbonates is an excellent archive of the geochemical conditions under which they formed (Greinert et al., 2001; Naehr et al., 2007; Peckmann et al., 2001b; Pierre et al., 2012). The stable carbon and oxygen isotopic composition of seep carbonates serves as an indicator of the composition and source of seep fluids (e.g. Chen et al., 2005, 2007; Feng et al., 2008; Peckmann et al., 2001b; Peckmann and Thiel, 2004; Roberts et al., 2010; Roberts and Aharon, 1994). Seep carbonates from GC140 are mainly composed of aragonite and HMC, with minor amounts of LMC and dolomite (Table 1). However, distinct mineralogical constituents exist in different types of carbonates. The samples exhibit a wide range of carbon and oxygen isotopic

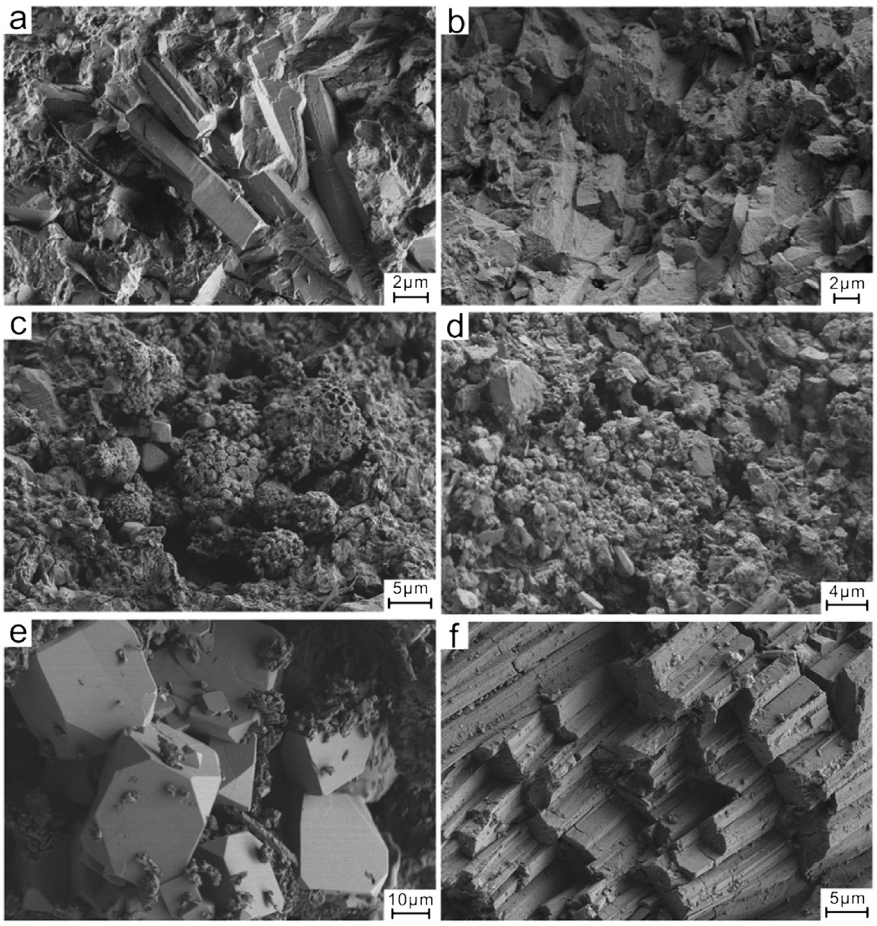

Figure 4. Scanning electron micrographs of seep carbonates. (a) Co-occurrence of acicular aragonite and micritic Mg-calcite, sample 4-a of Structure I carbonates. (b) Mg-calcite crystals in 4-a of Structure I carbonates. (c) Framboidal pyrites in the matrix of B-10 of Structure I carbonates. (d) The crystals of Mg-calcite in the matrix bioclastic carbonates, sample B-11 of Structure II carbonates. (e) Well developed crystals of NaCl in B-12 of Structure II carbonates. (f) Fibrous aragonite in F-2 of Structure III carbonates.

compositions, indicating complex fluid sources and varied formation conditions.

The carbonate mineralogy of Structure I carbonates is characterized by HMC, aragonite, and dolomite. The most common mineral is HMC, suggesting formation in the subsurface with relative low sulfate content (cf. Greinert et al., 2001). The $\delta^{13}C$ values of the carbonates vary between −23.2‰ and 5.1‰, suggesting multiple carbon sources that include seawater, thermogenic methane, biodegraded crude oil and residual CO_2 from methanogenesis. Moreover, the positive $\delta^{13}C$ values (up to 5.1‰) are similar to the carbon isotopic values (14‰) of seep carbonates from Alaminos Canyon 601 of the GOM, indicating formation in deeper sediment (Roberts et al., 2010). This interpretation is also supported by the presence of dolomite, which usually occurs within the subsurface (cf. Naehr et al., 2007; Peckmann et al., 1999).

Structure II carbonates are dominated by HMC and aragonite with a minor amount of LMC. The precipitation of LMC may be associated with brine seepage. It is suggested that the GOM brine has a low Mg/Ca ratio (<1) and with low concentrations of sulfide and little to no sulfate (cf. Feng and Roberts, 2011; Joye et al., 2005). This interpretation is also supported by the occurrence of NaCl with well-developed crystals. There is no structure indicating recrystallization based on the thin section observation. It is suggested that the LMC is primary instead of resulting from recrystallization of HMC or aragonite. Slightly negative carbon isotopic ratios (−22.2‰ to −8.8‰) suggest that thermogenic gas from a deep hydrocarbon reservoir appears to be the primary carbon source.

The aragonite dominated Structure III carbonates represent precipitation at a place very close to or directly at the seafloor, where HCO_3^--rich fluids generated by anaerobic methane oxidation mixed with sulfate-rich bottom seawater. Luff and Wallmann (2003) suggested that the occurrence of aragonite reflects a high methane flux and efficient methane oxidation, resulting in low $\delta^{13}C$ carbonate values. The $\delta^{13}C$ values of the carbonates vary from −36.1‰ to −26.8‰, suggesting that the carbon is almost entirely from thermogenic methane.

The oxygen isotopic composition provides information on the temperature and fluid source from which the seep carbonate precipitated (Anderson and Arthur, 1983; Stakes et al., 1999). The $\delta^{18}O$ values of the Structure I carbonates and Structure II carbonates are slightly above the values precipitated in equilibrium with the present bottom water temperature (Fig. 5), suggesting the addition of a certain amount of ^{18}O-enriched fluid into the pore fluid apart from seawater. The decomposition of gas hydrate as the cause of the ^{18}O-enriched fluid is precluded because the pressure and temperature conditions were not favorable to the formation of gas hydrate at GC140. Thus, we propose that the ^{18}O-enriched fluid was released by conversion of smectite to illite at greater depths (Hesse, 2003). The ^{18}O-enriched fluid was transported to the seabed through the cold seep plumping system, and this signal was finally preserved in the associated authigenic carbonate. Additionally, small amounts of dolomite in the Structure I carbonates may have contributed to the elevated oxygen isotopic composition. The $\delta^{18}O$ value of dolomite is about 3‰ more positive than that of the

Table 2
Stable carbon and oxygen isotopic compositions of the seep carbonates.

Sample no.	Sub-sample ID	$\delta^{13}C$/‰	$\delta^{18}O$/‰	Note
Structure I carbonates				
4-a	1	−12.3	3.0	Nodule
	2	−3.9	3.4	Nodule
	3	−17.7	2.8	Nodule
	4	−16.0	3.0	Matrix
	5	−20.1	3.1	Matrix
	6	1.4	3.1	Matrix
	7	−23.2	2.9	Matrix
	8	−2.5	3.2	Matrix
	9	−19.8	2.8	Matrix
B-10	1	−18.7	2.2	Nodule
	2	−13.0	2.8	Nodule
	3	−9.8	2.8	Nodule
	4	−11.1	2.9	Nodule
	5	3.3	2.6	Matrix
	6	−2.8	2.5	Matrix
	7	0.8	2.4	Matrix
	8	−0.9	2.9	Matrix
B-9	1	5.1	3.0	Nodule
	2	−1.8	3.3	Nodule
	3	1.3	3.2	Nodule
	4	−10.5	2.5	Nodule
	5	−13.2	3.2	Matrix
Structure II carbonates				
B-11	1	−11.4	2.5	Matrix
	2	−8.8	2.6	Matrix
	3	−15.1	2.0	Matrix
	4	−22.2	2.7	Matrix
B-12	1	−11.5	2.9	Matrix
	2	−14.7	3.1	Matrix
	3	−14.0	2.8	Matrix
B-3	1	−16.3	3.5	Nodule
	2	−16.7	2.8	Nodule
	3	−16.8	2.9	Matrix
	4	−15.3	2.7	Matrix
	5	−10.9	3.3	Matrix
	6	−16.6	3.1	Matrix
Structure III carbonates				
F-2	1	−33.1	2.2	Matrix
	2	−31.0	2.4	Matrix
	3	−29.9	2.4	Matrix
	4	−26.8	2.1	Matrix
	5	−31.9	2.7	Matrix
	6	−36.1	1.9	Matrix
	7	−35.6	2.5	Aragonite in pore
	8	−34.8	2.6	Aragonite in pore

coprecipitated calcite (Land, 1980). The $\delta^{18}O$ values of the aragonite-based Structure III carbonates are close to the theoretical values, representing precipitation in equilibrium with the bottom water at the present temperature (Fig. 5).

5.2. ^{14}C ages and episodical activity of the cold seep

Recently, chronology combined with mineralogy, petrology, stable isotopes, and trace element geochemistry have been applied to shed light on the evolution of seep activity (Aharon et al., 1997; Bayon et al., 2009a,b; Feng et al., 2010b; Kutterolf et al., 2008; Liebetrau et al., 2010; Teichert et al., 2003; Watanabe et al., 2008). For example, U/Th ages of seep carbonates from Hydrate Ridge show that the occurrence of seep carbonate appears to have been correlated with the sea level lowstand during Pleistocene glacial–interglacial cycles (Teichert et al., 2003). Seeps have been particularly active during the last glaciation in the GOM and Sea of Japan (Feng et al., 2010b; Kutterolf et al., 2008; Watanabe et al., 2008).

Aharon et al. (1997) reported that the hydrocarbon seeps in the GOM have been active since the late Pleistocene. In addition, Roberts et al. (1990) and Feng et al. (2010b) showed that the GOM

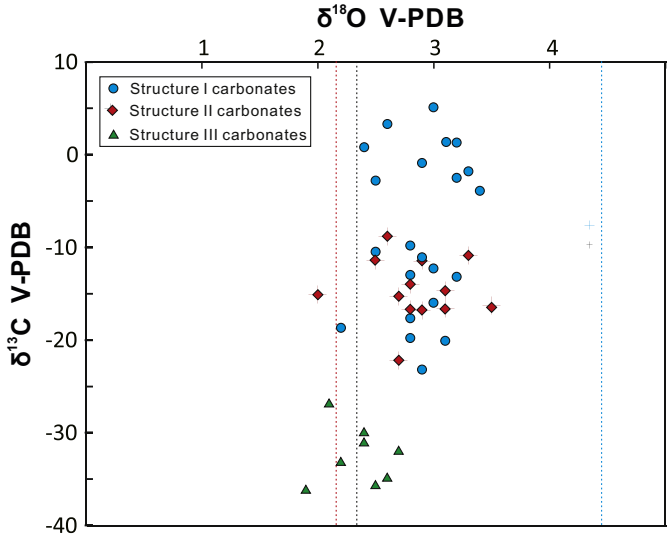

Figure 5. Stable carbon and oxygen isotopic compositions of seep carbonates. The dashed lines indicate the theoretical $\delta^{18}O$ values for HMC (2.16‰; red), aragonite (2.32‰; black) and dolomite (4.46‰; blue) precipitating in equilibrium with bottom water at the present temperature (t = 12.87 °C, $\delta^{18}O$ = 0.7‰ SMOW). The calculations were made based on the equations of Friedman and O'Neil (1977), Hudson and Anderson (1989) and Fritz and Smith (1970) for Mg-calcite, aragonite and dolomite, respectively. The mol% $MgCO_3$ content of Mg-calcite is assumed to be 13.5% (Table 1).

hydrocarbon seeps are not continually active. The latter authors proposed that the current phase of vigorous seepage at the lower continental slope began at approximately 12.4 ka BP, possibly reflecting a time of increased sedimentary loading and associated salt diapirism that activated fault conduits to the seafloor at the end of the last deglaciation.

The ^{14}C dating of the shells suggests that GC140 seep carbonates formed during three different time intervals, revealing that fluid seepage at this site occurred episodically. The ^{14}C ages of the three structures are 46.5 ka to 25.8 ka BP, 17.6 ka to 11.7 ka BP, and 1.2 ka BP, respectively (Table 3 and Fig. 6). In particular, ^{14}C ages of sample B-10 from Structure I show a wide range with ^{14}C ages of between 41.3 ka and 5.0 ka BP, which may be due to multiple stages (Fig. 6). It is suggested that the enhanced fluid flow during these time intervals was closely related to not only the sea level variations associated with glacial/interglacial cycles but also the salt tectonics. Interestingly, the different orientations of the geopetal structures in

Table 3
^{14}C dating results of bivalve shells cemented by seep carbonates.

Sample no.	$\delta^{13}C$/‰	^{14}C age (a BP[a])	^{14}C age (corrected, a BP)
Structure I carbonates			
4-a-1	2.8	33,610 ± 170	34,068 ± 170
4-a-2	3.4	46,010 ± 580	46,479 ± 580
4-a-3	3.2	31,470 ± 150	31,936 ± 150
4-a-4	−2.9	25,790 ± 110	26,153 ± 110
B-10-1	2.7	4500 ± 30	4957 ± 30
B-10-2	2.2	40,900 ± 480	41,348 ± 480
B-10-3	2.7	35,620 ± 220	36,078 ± 220
B-9	3.8	25,330 ± 100	25,807 ± 100
Structure II carbonates			
B-11	3.2	11,210 ± 60	11,675 ± 60
B-12-1	0.6	14,315 ± 50	14,736 ± 50
B-12-2	1.8	17,140 ± 80	17,583 ± 80
B-12-3	1.0	13,960 ± 60	14,388 ± 60
B-3	3.7	17,070 ± 60	17,545 ± 60
Structure III carbonates			
F-2-1	2.2	800 ± 25	1249 ± 25
F-2-2	2.3	750 ± 25	1201 ± 25

[a] BP = before present, years from 1950 AD.

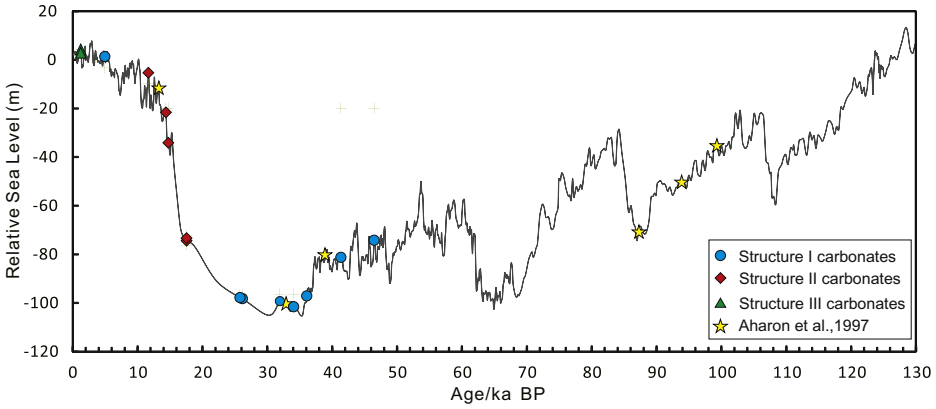

Figure 6. The AMS ^{14}C ages for samples of bivalve shell materials cemented in GC140 seep carbonates. The sea level curve derived from oxygen isotope data is a proxy for the eustatic sea level change over the past 130 ka (Rohling et al., 2009).

an authigenic carbonate rock from GC140 indicate multiple reworking, most likely resulting from salt tectonics in this area (Roberts, 2001).

Salt tectonics involving the evolution of various salt body geometries including salt diapirs are common to the northern Gulf of Mexico (Cook and D'Onfro, 1991; Seni, 1992; Sassen et al., 1999). Submersible observations and high resolution acoustic datasets show that faults are widespread in sediments as a result of tectonic activity (Roberts et al., 1990, 1993, 2000), suggesting that the movement of salt has been active. Therefore, the possible factors governing the episodical intensification of the seep activity in the studied area are sea level change, sedimentary loading, and salt movement.

5.3. The evolution of seep fluids at GC140

In the GOM, the dynamic fluid flow along deformed salt bodies and faults causes the rapid expulsion of fluid and gas and provides conditions suitable for the formation of authigenic carbonates close to the seafloor (Roberts, 2001, 2011). The carbonate outcropping at the seafloor consequently provides an accessible overview to monitor the long-term dynamics of fluid and gas expulsions. By integrating mineralogical and geochemical data and ^{14}C ages, a schematic model of the evolution of seep fluids at GC140 is proposed (Fig. 7).

In Stage I (from 46.5 ka to 25.8 ka BP), low flux of fluid seepage at the studied location led to the formation of Structure I carbonates. The presence of HMC and dolomite mineral phases in the samples suggests that the precipitation of Structure I carbonates occurred in relatively deeper sediments. This assumption is supported by positive $\delta^{13}C$ values (up to 5.1‰) of Structure I carbonates, which represent precipitation resulting from methanogenesis deeper within the deep sediment. The presence of small amounts of LMC in one sample of Structure I (sample B-10) suggests the influence of locally active brine seepage (cf. Feng and Roberts, 2011).

In Stage II (from 17.6 ka to 11.7 ka BP), intermediate fluid seepage promoted the formation of Structure II carbonates. The presence of fragments of shells of chemosynthetic bivalves in the carbonates suggests that the carbonate precipitation during this stage occurred close to the seafloor. The presence of LMC in the carbonates suggests the influence of brines during its formation (cf. Feng and Roberts, 2011).

In Stage III (from ~1.2 ka BP to present), the enhanced fluid flow induced the formation of Structure III carbonates. The aragonitic mineralogy of the carbonates is indicative of precipitation in a sulfate-rich environment. Moreover, the $\delta^{18}O$ values close to the

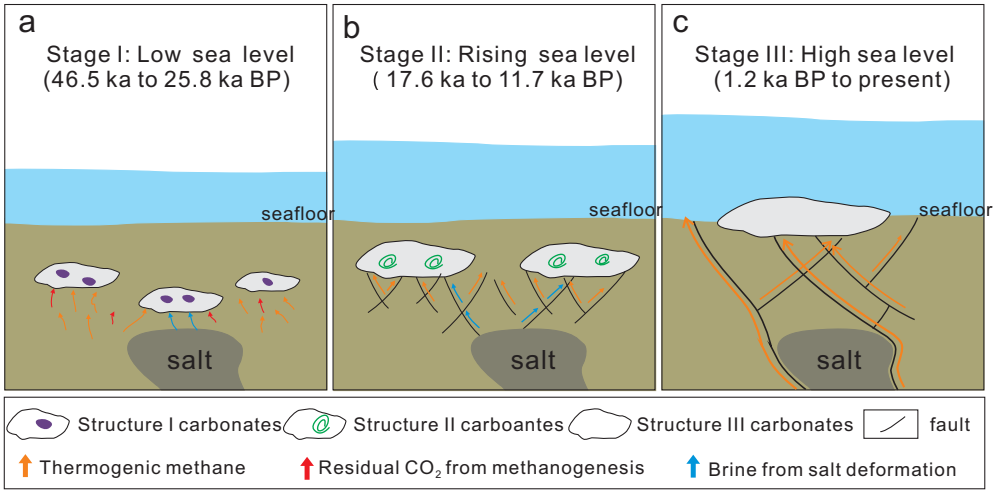

Figure 7. Schematic model illustrating the evolution of seep fluids. (a) Stage I (from 46.5 ka to 25.8 ka BP): sea level lowstand. The salt body at the studied site was inactive. Slow fluid seeping lead to precipitation of carbonate of Structure I carbonates in relatively deeper sediment; (b) Stage II (from 17.6 ka to 11.7 ka BP): the sea level was rising. The salts began to be active and brought some brine for the precipitation of LMC, Structure II carbonates; (c) Stage III (from ~1.2 ka BP to present): sea level highstand. The salt deformation was aggravated and broke upper sediment, which formed aragonite-based carbonates of Structure III carbonates near or at the seafloor.

calculated equilibrium values agree with precipitation from pore waters with a composition close to that of the seawater. Additionally, the high methane flux results in relatively negative $\delta^{13}C$ values of the carbonates (cf. Luff and Wallmann, 2003). Overall, our results suggest that the evolution of fluids at cold seeps is a dynamic process. This variability most likely reflects changes in the seepage flux that are linked to multiple factors such as sea level changes, sedimentation, and salt deformation. The combination of petrographic and geochemical constraints as well as the detailed chronology used here is promising to better assess the variability and the diversity of past fluid and gas expulsions at seeps.

6. Conclusion

The authigenic carbonate rocks collected from Green Canyon block 140, northern Gulf of Mexico, provided information on the site specific evolution of seep fluids and the possible driving forces. Three structures of carbonate cements were recognized based on different cement types. They consist of a variety of carbonate mineral phases including high-Mg calcite, aragonite, low-Mg calcite, and dolomite. The occurrence of different types of carbonates and the large variation in $\delta^{13}C$ values appear to be closely related to the intensity of the seepage and the involvement of brines from salt dissolution. Structure I carbonates with ^{14}C ages between 46.5 ka and 25.8 ka BP are suggested to have formed in deeper sediment, agreeing with the apparent positive $\delta^{13}C$ values as high as 5.1‰ and the presence of the dolomite mineral phase. The fluid flux during this time interval was low. Structure II carbonates formed from 17.6 ka to 11.7 ka BP. The precipitation occurred close to the seafloor in the shallow subsurface due to the moderate fluid flow as revealed by abundant bivalve shell fragments in the carbonates. The involvement of brines is suggested by the presence of low-Mg calcite. Aragonitic Structure III carbonates formed at higher methane concentrations correspond to enhanced fluid flow as indicated by negative $\delta^{13}C$ values as low as −36.1‰. The findings also emphasize that the factors influencing seep activity are not only sea level changes and sedimentation, but also salt tectonics. This study reveals that authigenic carbonates have the potential to archive the long-term evolution of fluid flow at hydrocarbon seeps.

Acknowledgments

The seep carbonates analyzed in this study were obtained on the cruises sponsored by the Bureau of Ocean Energy Management (BOEM; formerly Minerals Management Service). The study was partially supported by the Knowledge Innovation Program of CAS (KZCX2-YW-GJ03), the NSF of China (Grants: 91228206 and 91028012), “Hundred Talents Program” of CAS, and GIGCAS 135 project Y234021001. We are grateful to Drs. C. Shen and F. Wang (both GIG, CAS) for technical assistance during the experiments. Furthermore, we thank Editor Dr. P. Gianolla, reviewer Dr. A. Mazzini and one anonymous reviewer for their helpful comments that greatly improved an earlier version of this manuscript. This is contribution No. IS-1653 from GIGCAS.

References

Aharon, P., 1994. Geology and biology of modern and ancient submarine hydrocarbon seeps and vents: an introduction. Geo-Marine Letters 14, 69–73.

Aharon, P., Schwarcz, H.P., Roberts, H.H., 1997. Radiometric dating of submarine hydrocarbon seeps in the Gulf of Mexico. Geological Society of America Bulletin 109, 568–579.

Aloisi, G., Pierre, C., Rouchy, J., Foucher, J., Woodside, J., Party, M.S., 2000. Methane-related authigenic carbonates of eastern Mediterranean Sea mud volcanoes and their possible relation to gas hydrate destabilisation. Earth and Planetary Science Letters 184, 321–338.

Anderson, T.F., Arthur, M.A., 1983. Stable isotopes of oxygen and carbon and their application to sedimentologic and paleoenvironmental problems. In: Sedimentary Geology. Society of Economic Paleontologists and Mineralogists, Dallas. pp. 1–151.

Baker, P.A., Burns, S.J., 1985. Occurrence and formation of dolomite in organic-rich continental margin sediments. American Association of Petroleum Geologists Bulletin 69, 1917–1930.

Bayon, G., Birot, D., Ruffine, L., Caprais, J.C., Ponzevera, E., Bollinger, C., Donval, J.P., Charlou, J.L., Voisset, M., Grimaud, S., 2011. Evidence for intense REE scavenging at cold seeps from the Niger Delta margin. Earth and Planetary Science Letters 312, 443–452.

Bayon, G., Henderson, G.M., Bohn, M., 2009a. U–Th stratigraphy of a cold seep carbonate crust. Chemical Geology 260, 47–56.

Bayon, G., Loncke, L., Dupré, S., Caprais, J.C., Ducassou, E., Duperron, S., Etoubleau, J., Foucher, J.P., Fouquet, Y., Gontharet, S., Henderson, G.M., Huguen, C., Klaucke, I., Mascle, J., Migeon, S., Roy, K.O., Ondréas, H., Pierre, C., Sibuet, M., Stadnitskaia, A., Woodside, J., 2009b. Multi-disciplinary investigation of fluid seepage on an unstable margin: the case of the Central Nile deep sea fan. Marine Geology 261, 92–104.

Bayon, G., Pierre, C., Etoubleau, J., Voisset, M., Cauquil, E., Marsset, T., Sultan, N., Le Drezen, E., Fouquet, Y., 2007. Sr/Ca and Mg/Ca ratios in Niger Delta sediments: implications for authigenic carbonate genesis in cold seep environments. Marine Geology 241, 93–109.

Berner, R.A., 1980. Early Diagenesis – a Theoretical Approach. Princeton University Press, Princeton, New Jersey, USA. pp. 1–241.

Birgel, D., Feng, D., Roberts, H.H., Peckmann, J., 2011. Changing redox conditions at cold seeps as revealed by authigenic carbonates from Alaminos Canyon, northern Gulf of Mexico. Chemical Geology 285, 82–96.

Boetius, A., Ravenschlag, K., Schubert, C.J., Rickert, D., Widdel, F., Gieseke, A., Amann, R., Jørgensen, B.B., Witte, U., Pfannkuche, O., 2000. A marine microbial consortium apparently mediating anaerobic oxidation of methane. Nature 407, 623–626.

Bohrmann, G., Greinert, J., Suess, E., Torres, M., 1998. Authigenic carbonates from the Cascadia subduction zone and their relation to gas hydrate stability. Geology 26, 647–650.

Burton, E.A., 1993. Controls on marine carbonate cement mineralogy: review and reassessment. Chemical Geology 105, 163–179.

Burton, E.A., Walter, L.M., 1991. The effects of PCO_2 and temperature on magnesium incorporation in calcite in seawater and $MgCl_2$-$CaCl_2$ solutions. Geochimica et Cosmochimica Acta 55, 777–785.

Campbell, K.A., 2006. Hydrocarbon seep and hydrothermal vent paleoenvironments and paleontology: past developments and future research directions. Palaeogeography, Palaeoclimatology, Palaeoecology 232, 362–407.

Campbell, K.A., Nelson, C.S., Alfaro, A.C., Boyd, S., Greinert, J., Nyman, S., Grosjean, E., Logan, G.A., Gregory, M.R., Cooke, S., Linke, P., Milloy, S., Wallis, I., 2010. Geological imprint of methane seepage on the seabed and biota of the convergent Hikurangi Margin, New Zealand: box core and grab carbonate results. Marine Geology 272, 285–306.

Chen, D., Cathles, L.M., Roberts, H.H., 2004. The geochemical signatures of variable gas venting at gas hydrate sites. Marine and Petroleum Geology 21, 317–326.

Chen, D., Feng, D., Su, Z., Song, Z.G., Chen, G.Q., Cathles, L.M., 2006. Pyrite crystallization in seep carbonates at gas vent and hydrate site. Materials Science and Engineering: C 26, 602–605.

Chen, D., Huang, Y.Y., Yuan, X.L., Cathles, L.M., 2005. Seep carbonates and preserved methane oxidizing archaea and sulfate reducing bacteria fossils suggest recent gas venting on the seafloor in the Northeastern South China Sea. Marine and Petroleum Geology 22, 613–621.

Chen, D., Liu, Q., Zhang, Z., Cathles, L.M., Roberts, H.H., 2007. Biogenic fabrics in seep carbonates from an active gas vent site in Green Canyon Block 238, Gulf of Mexico. Marine and Petroleum Geology 24, 313–320.

Cook, D., D'Onfro, P., 1991. Jolliet field thrust fault structure and stratigraphy Green Canyon block 184, offshore Louisiana. Transactions Gulf Coast Association of Geological Societies 41, 100–121.

Dahlmann, A., de Lange, G.J., 2003. Fluid-sediment interactions at Eastern Mediterranean mud volcanoes: a stable isotope study from ODP Leg 160. Earth and Planetary Science Letters 212, 377–391.

Davidson, D.W., Leaist, D.G., Hesse, R., 1983. Oxygen-18 enrichment in the water of a clathrate hydrate. Geochimica et Cosmochimica Acta 47, 2293–2295.

Davis, K.J., 2000. The role of Mg^{2+} as an impurity in calcite growth. Science 290, 1134–1137.

Díaz-del-Río, V., Somoza, L., Martínez-Frias, J., Mata, M.P., Delgado, A., Hernandez-Molina, F.J., Lunar, R., Martín-Rubí, J.A., Maestro, A., Fernández-Puga, M.C., León, R., Llave, E., Medialdea, T., Vázquez, J.T., 2003. Vast fields of hydrocarbon-derived carbonate chimneys related to the accretionary wedge/olistostrome of the Gulf of Cádiz. Marine Geology 195, 177–200.

Feng, D., Chen, D., Peckmann, J., 2009a. Rare earth elements in seep carbonates as tracers of variable redox conditions at ancient hydrocarbon seeps. Terra Nova 21, 49–56.

Feng, D., Chen, D., Peckmann, J., Bohrmann, G., 2010a. Authigenic carbonates from methane seeps of the northern Congo fan: microbial formation mechanism. Marine and Petroleum Geology 27, 748–756.

Feng, D., Chen, D., Roberts, H.H., 2008. Sedimentary fabrics in the authigenic carbonates from Bush Hill: implication for seabed fluid flow and its dynamic signature. Geofluids 8, 301–310.

Feng, D., Chen, D., Roberts, H.H., 2009b. Petrographic and geochemical characterization of seep carbonate from Bush Hill (GC 185) gas vent and hydrate site of the Gulf of Mexico. Marine and Petroleum Geology 26, 1190–1198.
Feng, D., Roberts, H.H., 2011. Geochemical characteristics of the barite deposits at cold seeps from the northern Gulf of Mexico continental slope. Earth and Planetary Science Letters 309, 89–99.
Feng, D., Roberts, H.H., Cheng, H., Peckmann, J., Bohrmann, G., Lawrence Edwards, R., Chen, D., 2010b. U/Th dating of cold-seep carbonates: an initial comparison. Deep Sea Research Part II: Topical Studies in Oceanography 57, 2055–2060.
Friedman, I., O'Neil, J.R., 1977. Compilation of stable isotope fractionation factors of geochemical interest. In: Fleishcher, M. (Ed.), Data of Geochemistry, sixth ed. US Geol. Survey Professional Paper 440–KK.
Fritz, P., Smith, D.G.W., 1970. Isotopic composition of secondary dolomites. Geochimica et Cosmochimica Acta 34, 1161–1173.
Gieskes, J., Mahn, C., Day, S., Martin, J., Greinert, J., Rathburn, T., McAdoo, B., 2005. A study of the chemistry of pore fluids and authigenic carbonates in methane seep environments: Kodiak Trench, Hydrate Ridge, Monterey Bay, and Eel River Basin. Chemical Geology 220, 329–345.
Goldsmith, J.R., Graf, D.L., Heard, H.C., 1961. Lattice constants of the calcium–magnesium carbonates. American Mineralogist 46, 453–457.
Greinert, J., 2008. Monitoring temporal variability of bubble release at seeps: the hydroacoustic swath system GasQuant. Journal of Geophysical Research 113. http://dx.doi.org/10.1029/2007JC004704.
Greinert, J., Bohrmann, G., Suess, E., 2001. Gas hydrate-associated carbonates and methane-venting at Hydrate Ridge: classification, distribution and origin of authigenic lithologies. In: Paull, C.K., Dillon, W.P. (Eds.), Natural Gas Hydrates: Occurrence, Distribution, and Detection. Geophysical Monographs, vol. 124. American Geophysical Union, Washington, DC, pp. 99–113.
Greinert, J., Bollwerk, S.M., Derkachev, A., Bohrmann, G., Suess, E., 2002. Massive barite deposits and carbonate mineralization in the Derugin Basin, Sea of Okhotsk: precipitation process at cold vent sites. Earth and Planetary Science Letters 203, 165–180.
Greinert, J., Derkachev, A., 2004. Glendonites and methane-derived Mg-calcites in the Sea of Okhotsk, Eastern Siberia: Implications of a venting-related ikaite/glendonite formation. Marine Geology 204, 129–144.
Hesse, R., 2003. Pore water anomalies of submarine gas-hydrate zones as tool to assess hydrate abundance and distribution in the subsurface what have we learned in the past decade? Earth-Science Reviews 61, 149–179.
Hudson, J.C., Anderson, T.F., 1989. Ocean temperatures and isotopic compositions through time. In: Clarkson, E.N.K., Curry, G.B., Rolfe, W.D.I. (Eds.), Environments and Physiology of Fossil Organisms. Transactions Royal Society of Edinburgh: Earth Sciences, vol. 80, pp. 183–192.
Ivanov, M., Mazzini, A., Blinova, V., Kozlova, E., Laberg, J.-S., Matveeva, T., Taviani, M., Kaskov, N., 2010. Seep mounds on the Southern Vøring Plateau (offshore Norway). Marine and Petroleum Geology 27, 1235–1261.
Joye, S.B., MacDonald, I.R., Montoya, J.P., Peccini, M., 2005. Geophysical and geochemical signatures of Gulf of Mexico seafloor brines. Biogeosciences 2, 295–309.
Judd, A.G., Hovland, M., 2007. Seabed Fluid Flow Impact on Geology Biology, and the Marine Environment. Cambridge University Press, Cambridge, UK. pp. 1–475.
Kutterolf, S., Liebetrau, V., Morz, T., Freundt, A., Hammerich, T., Garbe-Schonberg, D., 2008. Lifetime and cyclicity of fluid venting at forearc mound structures determined by tephrostratigraphy and radiometric dating of authigenic carbonates. Geology 36, 707–710.
Land, L.S., 1980. The isotopic and trace element geochemistry of dolomite: the state of the art. In: Zenger, D.H., Dunham, J.B., Ethington, R.L. (Eds.), Concepts and Models of Dolomitization, vol. 28. SEPM, pp. 87–110.
Liebetrau, V., Eisenhauer, A., Linke, P., 2010. Cold seep carbonates and associated cold-water corals at the Hikurangi Margin, New Zealand: new insights into fluid pathways, growth structures and geochronology. Marine Geology 272, 307–318.
Luff, R., Wallmann, K., 2003. Fluid flow, methane fluxes, carbonate precipitation and biogeochemical turnover in gas hydrate-bearing sediments at Hydrate Ridge, Cascadia Margin: numerical modeling and mass balances. Geochimica et Cosmochimica Acta 67, 3403–3421.
Lumsden, D.N., 1979. Error in X-ray diffraction estimates of dolomite in carbonate rocks—causes and cures. American Association of Petroleum Geologists Bulletin 63, 488.
MacDonald, I.R., Smith, M., Huffer, F.W., 2010. Community structure comparisons of lower slope hydrocarbon seeps, northern Gulf of Mexico. Deep Sea Research Part II: Topical Studies in Oceanography, 1904–1915.
Magalhães, V.H., Pinheiro, L.M., Ivanov, M.K., Kozlova, E., Blinova, V., Kolganova, J., Vasconcelos, C., McKenzie, J.A., Bernasconi, S.M., Kopf, A.J., Díaz-del-Río, V., González, F.J., Somoza, L., 2012. Formation processes of methane-derived authigenic carbonates from the Gulf of Cadiz. Sedimentary Geology 243–244, 155–168.
Matsumoto, R.Y.O., 1994. Methane hydrate estimates from the chloride and oxygen isotopic anomalies: examples from the Blake Ridge and Nankai Trough Sediments. Annals of the New York Academy of Sciences 912, 39–50.
Mazzini, A., Aloisi, G., Akhmanov, G.G., Parnell, J., Cronin, B.T., Murphy, P., 2005. Integrated petrographic and geochemical record of hydrocarbon seepage on the Voring Plateau. Journal of the Geological Society, London 162, 815–827.
Mazzini, A., Ivanov, M.K., Nermoen, A., Bahr, A., Borhmann, G., Svensen, H., Planke, S., 2008. Complex plumbing systems in the near subsurface: geometries of authigenic carbonates from Dolgovskoy Mound (Black Sea) constrained by analogue experiments. Marine and Petroleum Geology 25, 457–472.
Mazzini, A., Ivanov, M.K., Parnell, J., Stadnitskaya, A., Cronin, B., Poludetkina, E., Mazurenko, L., van Weering, T.C.E., 2004. Methane-related authigenic carbonates from the Black Sea: geochemical characterization and relation to seeping fluids. Marine Geology 212, 153–181.
Mazzini, A., Svensen, H., Hovland, M., Planke, S., 2006. Comparison and implications from strikingly different authigenic carbonates in a Nyegga complex pockmark, G11, Norwegian Sea. Marine Geology 231, 89–102.
Milkov, A.V., Sassen, R., 2001. Estimate of gas hydrate resource, northwestern Gulf of Mexico continental slope. Marine Geology 179, 71–83.
Moore, T.S., Murray, R.W., Kurtz, A.C., Schrag, D.P., 2004. Anaerobic methane oxidation and the formation of dolomite. Earth and Planetary Science Letters 229, 141–154.
Naehr, T.H., Eichhubl, P., Orphan, V.J., Hovland, M., Paull, C.K., Ussler, W., Lorenson, T.D., Greene, H.G., 2007. Authigenic carbonate formation at hydrocarbon seeps in continental margin sediments: a comparative study. Deep Sea Research Part II: Topical Studies in Oceanography 54, 1268–1291.
Naehr, T.H., Rodriguez, N.M., Bohrmann, G., Paull, C.K., Botz, R., 2000. Methane derived authigenic carbonates associated with gas hydrate decomposition and fluid venting above the Blake Ridge Diapir. In: Paull, C.K., Matsumoto, R., Wallace, P.J., Dillon, W.P. (Eds.), Proceedings of the Ocean Drilling Program, Scientific Results, vol. 164, pp. 285–300.
Paull, C.K., Martens, C.S., Chanton, J.P., Neumann, A.C., Coston, J., Jull, A.J.T., Toolin, L.J., 1989. Old carbon in living organisms and young $CaCO_3$ cements from abyssal brine seeps. Nature 342, 166–168.
Paull, C.K., Ussler, W., Peltzer, E.T., Brewer, P.G., Keaten, R., Mitts, P.J., Nealon, J.W., Greinert, J., Herguera, J.-C., Elena Perez, M., 2007. Authigenic carbon entombed in methane-soaked sediments from the northeastern transform margin of the Guaymas Basin, Gulf of California. Deep Sea Research Part II: Topical Studies in Oceanography 54, 1240–1267.
Peckmann, J., Birgel, D., Kiel, S., 2009. Molecular fossils reveal fluid composition and flow intensity at a Cretaceous seep. Geology 37, 847–850.
Peckmann, J., Gischler, E., Oschmann, W., Reitner, J., 2001a. An early carboniferous seep community and hydrocarbon-derived carbonates from the Harz Mountains, Germany. Geology 29, 271–274.
Peckmann, J., Goedert, J.L., Thiel, V., Michaelis, W., Reitner, J., 2002. A comprehensive approach to the study of methane-seep deposits from the Lincoln Creek Formation, western Washington State, USA. Sedimentology 49, 855–873.
Peckmann, J., Reimer, A., Luth, U., Luth, C., Hansen, B.T., Heinicke, C., Hoefs, J., Reitner, J., 2001b. Methane-derived carbonates and authigenic pyrite from the northwestern Black Sea. Marine Geology 177, 129–150.
Peckmann, J., Thiel, V., 2004. Carbon cycling at ancient methane-seeps. Chemical Geology 205, 443–467.
Peckmann, J., Thiel, V., Michaelis, W., Clari, P., Gaillard, C., Martire, L., Reitner, J., 1999. Cold seep deposits of Beauvoisin (Oxfordian; southeastern France) and Marmorito (Miocene; northern Italy): microbially induced authigenic carbonates. International Journal of Earth Sciences 88, 60–75.
Pierre, C., Blanc-Valleron, M.M., Demange, J., Boudouma, O., Foucher, J.P., Pape, T., Himmler, T., Fekete, N., Spiess, V., 2012. Authigenic carbonates from active methane seeps offshore southwest Africa. Geo-Marine Letters 32, 501–513.
Roberts, H.H., 2001. Fluid and gas expulsion on the northern Gulf of Mexico continental slope: mud-prone to mineral-prone responses. In: Paull, C.K., Dillon, W.P. (Eds.), Natural Gas Hydrates: Occurrence, Distribution, and Detection. American Geophysical Union, Washington, DC, USA, pp. 145–161.
Roberts, H.H., 2011. Surficial geology of the northern Gulf of Mexico continental slope: impacts of fluid and gas expulsion. In: Buster, N.A., Holmes, W.C., Camp, D.K. (Eds.), Gulf of Mexico Origin, Waters, and Biota. Geology, vol. 3. Texas A&M University Press, Texas, pp. 209–228.
Roberts, H.H., Aharon, P., 1994. Hydrocarbon-derived carbonate buildups of the northern Gulf of Mexico continental slope: a review of submersible investigations. Geo-Marine Letters 14, 135–148.
Roberts, H.H., Aharon, P., Carney, R., Larkin, J., Sassen, R., 1990. Sea floor responses to hydrocarbon seeps, Louisiana continental slope. Geo-Marine Letters 10, 232–243.
Roberts, H.H., Aharon, P., Walsh, M.W., 1993. Cold-seep carbonates of the Louisiana continental slope to basin floor. In: Rezak, R., Lavoie, D.L. (Eds.), Carbonate Microfabrics: Frontiers in Sedimentary Geology. Springer-Verlag, New York, NY, USA, pp. 95–104.
Roberts, H.H., Carney, R.S., 1997. Evidence of episodic fluid, gas, and sediment venting on the northern Gulf of Mexico continental slope. Economic Geology 92, 863–879.
Roberts, H.H., Coleman, J., Jesse Hunt, J., Shedd, W.W., 2000. Surface amplitude mapping of 3-seismic for improved interpretations of seafloor geology and biology. Gulf Coast Association of Geological Societies Transactions 50, 495–504.
Roberts, H.H., Feng, D., Joye, S.B., 2010. Cold-seep carbonates of the middle and lower continental slope, northern Gulf of Mexico. Deep Sea Research Part II: Topical Studies in Oceanography 57, 2040–2054.
Rohling, E.J., Grant, K., Bolshaw, M., Roberts, A.P., Siddall, M., Hemleben, C., Kucera, M., 2009. Antarctic temperature and global sea level closely coupled over the past five glacial cycles. Nature Geoscience 2, 500–504.
Rongemaille, E., Bayon, G., Pierre, C., Bollinger, C., Chu, N.C., Fouquet, Y., Riboulot, V., Voisset, M., 2011. Rare earth elements in cold seep carbonates from the Niger delta. Chemical Geology 286, 196–206.
Sackett, W.M., 1978. Carbon and hydrogen isotope effects during thermo-catalytic production of hydrocarbons in laboratory simulation experiments. Geochimica et Cosmochimica Acta 42, 571–580.

Sassen, R., Joye, S., Sweet, S.T., DeFreitas, D.A., Milkov, A.V., MacDonald, I.R., 1999. Thermogenic gas hydrates and hydrocarbon gases in complex chemosynthetic communities, Gulf of Mexico continental slope. Organic Geochemistry 30, 485–497.

Sassen, R., Roberts, H.H., Carney, R., Milkov, A.V., DeFreitas, D.A., Lanoil, B., Zhang, C., 2004. Free hydrocarbon gas, gas hydrate, and authigenic minerals in chemosynthetic communities of the northern Gulf of Mexico continental slope: relation to microbial processes. Chemical Geology 205, 195–217.

Schneider von Deimling, J., Rehder, G., Greinert, J., McGinnnis, D.F., Boetius, A., Linke, P., 2011. Quantification of seep-related methane gas emissions at Tommeliten, North Sea. Continental Shelf Research 31, 867–878.

Seni, S.J., 1992. Evolution of salt structures during burial of salt sheets on the slope, northern Gulf of Mexico. Marine and Petroleum Geology 9, 452–468.

Solomon, E.A., Kastner, M., Jannasch, H., Robertson, G., Weinstein, Y., 2008. Dynamic fluid flow and chemical fluxes associated with a seafloor gas hydrate deposit on the northern Gulf of Mexico slope. Earth and Planetary Science Letters 270, 95–105.

Stakes, D.S., Orange, D., Paduan, J.B., Salamy, K.A., Maher, N., 1999. Cold-seeps and authigenic carbonate formation in Monterey Bay, California. Marine Geology 159, 93–109.

Teichert, B.M.A., Eisenhauer, A., Bohrmann, G., Haase-Schramm, A., Bock, B., Linke, P., 2003. U/Th systematics and ages of authigenic carbonates from Hydrate Ridge, Cascadia Margin: recorders of fluid flow variations. Geochimica et Cosmochimica Acta 67, 3845–3857.

Tong, H., Feng, D., Cheng, H., Yang, S., Wang, H., Min, A.G., Edwards, R.L., Chen, Z., Chen, D., 2013. Authigenic carbonates from seeps on the northern continental slope of the South China Sea: new insights into fluid sources and geochronology. Marine and Petroleum Geology 43, 260–271.

Torres, M.E., McManus, J., Hammond, D.E., de Angelis, M.A., Heeschen, K.U., Colbert, S.L., Tryon, M.D., Brown, K.M., Suess, E., 2002. Fluid and chemical fluxes in and out of sediments hosting methane hydrate deposits on Hydrate Ridge, OR, I: hydrological provinces. Earth and Planetary Science Letters 201, 525–540.

Tryon, M.D., 2004. Fluid and chemical cycling at Bush Hill: implications for gas- and hydrate-rich environments. Geochemistry Geophysics Geosystems 5, 12004. http://dx.doi.org/10.1029/2004GC000778.

Tryon, M.D., Brown, K.M., 2001. Complex flow patterns through Hydrate Ridge and their impact on seep biota. Geophysical Research Letters 28, 2863–2866.

Valentine, D.L., Reeburgh, W.S., 2000. New perspectives on anaerobic methane oxidation. Environmental Microbiology 2, 477–484.

Watanabe, Y., Nakai, S., Hiruta, A., Matsumoto, R., Yoshida, K., 2008. U-Th dating of carbonate nodules from methane seeps off Joetsu, Eastern Margin of Japan Sea. Earth and Planetary Science Letters 272, 89–96.

Weimer, P., Rowan, M.G., McBride, B.C., Kligfield, R., 1998. Evaluating the petroleum systems of the northern deep Gulf of Mexico through integrated basin analysis: an overview. American Association of Petroleum Geologists Bulletin 82, 865–877.

Whiticar, M.J., 1999. Carbon and hydrogen isotope systematics of bacterial formation and oxidation of methane. Chemical Geology 161, 291–314.

Whiticar, M.J., Faber, E., Schoell, M., 1986. Biogenic methane formation in marine and fresh water environments: CO_2 reduction *vs* acetate fermentation–isotope evidence. Geochimica et Cosmochimica Acta 50, 693–709.

Xu, X., Trumbore, S.E., Zheng, S., Southon, J.R., McDuffee, K.E., Luttgen, M., Liu, J.C., 2007. Modifying a sealed tube zinc reduction method for preparation of AMS graphite targets: reducing background and attaining high precision. Nuclear Instruments and Methods in Physics Research Section B: Beam Interactions with Materials and Atoms 259, 320–329.